tvst

Article

Structure-Function Mapping Using a Three-Dimensional Neuroretinal Rim Parameter Derived From Spectral Domain Optical Coherence Tomography Volume Scans

Ali Riza Cenk Celebi[1,2,*], Elli A. Park[3,*], Alice Chandra Verticchio Vercellin[1,4], Edem Tsikata[1], Ramon Lee[1,5], Eric Shieh[1,6], Hussein Antar[1,7], Madeline Freeman[1,8], Jing Zhang[9], Christian Que[1,10], Huseyin Simavli[1,11], Michael McClurkin[12], Rong Guo[13], Tobias Elze[12,14], Johannes F. de Boer[15], and Teresa C. Chen[1]

[1] Department of Ophthalmology, Glaucoma Service, Massachusetts Eye and Ear, Boston, MA, USA
[2] Department of Ophthalmology, Acibadem University School of Medicine, Istanbul, Turkey
[3] Boston University School of Medicine, Boston, MA, USA
[4] Istituto di Ricovero e Cura a Carattere Scientifico—Fondazione Bietti, Rome, Italy
[5] Department of Ophthalmology, University of Southern California, Los Angeles, CA, USA
[6] Jules Stein Eye Institute, University of California, Los Angeles, Los Angeles, CA, USA
[7] University of Massachusetts Medical School, Worcester, MA, USA
[8] Smith College School for Social Work, Northampton, MA, USA
[9] Peking University First Hospital, Beijing, China
[10] Department of Ophthalmology, University of East Ramon Magsaysay Memorial Medical Center, Quezon City, Philippines
[11] Kudret Eye Hospital, Istanbul, Turkey
[12] Harvard Medical School, Boston, MA, USA
[13] Department of Medicine Statistics Core, University of California, Los Angeles, Los Angeles, CA, USA
[14] Schepens Eye Research Institute, Boston, MA, USA
[15] LaserLaB Amsterdam, Department of Physics and Astronomy, Vrije Universiteit, Amsterdam, The Netherlands

Correspondence: Teresa C. Chen, Massachusetts Eye and Ear, Glaucoma Service, 243 Charles Street, Boston, MA 02114, USA. e-mail: teresa_chen@meei.harvard.edu

Purpose: To assess the structure-function relationship in glaucoma using Humphrey visual field (HVF) perimetry and a three-dimensional neuroretinal rim parameter derived from spectral domain optical coherence tomography (SD-OCT) volume scans.

Methods: Structure-function correlation was analyzed globally and regionally (four quadrants and four sectors). Structural data included peripapillary retinal nerve fiber layer (RNFL) thickness and minimum distance band (MDB) neuroretinal rim thickness, defined as the shortest distance between the inner cup surface and the outer retinal pigment epithelium/Bruch's membrane complex. Logarithmic regression analyses were performed and Pearson correlation coefficients determined to assess relationship strength.

Results: The study consisted of 102 open-angle glaucoma patients and 58 healthy subjects. The Pearson correlation coefficient for global MDB thickness ($R = 0.585$) was higher than for global RNFL thickness ($R = 0.492$), but the difference was not statistically significant ($P = 0.18$). The correlation coefficients for regional MDB thicknesses and corresponding HVF sensitivities were higher than those for regional RNFL thicknesses and HVF in six out of eight regions ($P = 0.08$ to 0.47). In the remaining two out of eight regions, the correlation coefficients were higher for RNFL thickness than for MDB thickness ($P = 0.15$ to 0.20).

Conclusions: Three-dimensional MDB neuroretinal rim thickness relates to visual function as strongly as the most commonly used SD-OCT parameter for glaucoma, two-dimensional peripapillary RNFL thickness.

Translational Relevance: This paper illustrates the potential for 3D OCT algorithms to improve in vivo imaging in glaucoma.

Introduction

Glaucoma is a progressive disease that causes structural and functional damage.[1] Most structure-function studies have focused on retinal nerve fiber layer (RNFL) thickness measurements and have used the Cirrus (Carl Zeiss Meditec, Inc., Dublin, CA, USA) and Spectralis (Heidelberg Engineering, Heidelberg, Germany) spectral domain optical coherence tomography (SD-OCT) machines.[2–10] These studies demonstrate only moderate correlation between Humphrey visual field (HVF) testing and SD-OCT RNFL thickness measurements, with correlation coefficients ranging from 0.203 to 0.726.[6,8,10–12] RNFL thickness and HVF testing may have limited structure-function correlation because 1) RNFL thickness measurements have artifact rates ranging from 15.2% to 58.5%,[4,13–15] 2) RNFL thinning may not occur at the same time as HVF loss, and 3) individual variability in healthy eyes may give rise to structure-function discordance in patients with glaucoma.[16]

Compared to RNFL structural measurements, newer 3D neuroretinal rim measurements may better reflect the structure-function changes that occur in glaucoma, because these parameters have fewer artifacts, with only 7.4% of scans affected[17] compared to 15.2% to 58.5%[13–15] of 2D RNFL thickness scans. Three-dimensional neuroretinal rim parameters have the additional benefit of having equal or better diagnostic capability for glaucoma compared to RNFL thickness.[16,18–24] The concept of a reference-plane independent 3D neuroretinal rim parameter was first described by Povazay and was published as Minimum Distance Mapping area.[24] This concept, renamed the minimum distance band (MDB), was later validated by Chen and de Boer, who were the first to demonstrate that neuroretinal rim thickness and not area had better correlation with clinical data (i.e., disc photos and visual fields).[21–23] The commercial iteration of this concept, termed the Bruch's membrane opening-minimum rim width (BMO-MRW) by Chauhan et al, thus focuses on neuroretinal rim thickness and not area.[18,25] These parameters differ in the scan protocol from which neuroretinal rim thickness and area are calculated. They also differ in the definitions of the OCT-based disc border, with the MDB defining the disc border as the retinal pigment epithelium–Bruch's membrane (RPE/BM) complex and the BMO-MRW defining the disc border as the BMO.

Using current commercially available neuroretinal rim software, neuroretinal rim structure-function studies have shown moderate correlation with HVF data. For example, using the Cirrus SD-OCT, Pollet-

Villard et al.[8] found correlation coefficient values that were higher for BMO-MRW compared to RNFL thickness (e.g., 0.658 vs. 0.598 for the inferior-temporal region, $P < 0.01$). In another study using the Spectralis SD-OCT, Muth et al. cited correlation coefficients ranging from 0.353 to 0.689 for global BMO-MRW; however, they did not compare BMO-MRW values with RNFL parameters.[26] Therefore, while commercially available BMO-MRW values derive either from low-density radial scans (i.e., Spectralis) or from scans without averaging (i.e., Cirrus), it is unknown whether an experimental high-density scan protocol with more averaging would improve structure-function correlation.

Therefore, we hypothesized that the 3D neuroretinal rim parameter, MDB thickness, will exhibit better structure-function correlation with HVF testing than RNFL thickness for two key reasons. First, the MDB thickness is derived from an experimental high-density 193 raster-line optic nerve volume scan, which contains more information than both the 2D RNFL thickness scan and the 24-line radial scan from which BMO-MRW derives. Second, the classic Garway-Heath structure-function map was originally designed for the neuroretinal rim,[27–29] and other maps such as the Kanamori and Wirtschafter maps were developed to better correlate RNFL changes with HVF changes.[30,31] To the best of our knowledge, this is the first study which uses the Garway-Heath structure-function map to correlate 3D MDB neuroretinal rim thickness with HVF testing in both normal and open-angle glaucoma patients.

Materials and Methods

Study Participants

All study participants were recruited from the Massachusetts Eye and Ear Glaucoma Service and imaged between January 2009 and January 2015 as a part of the ongoing prospective Spectral Domain OCT in Glaucoma study. The study protocol was approved by the Massachusetts Eye and Ear Institutional Review Board. Written informed consent was obtained from all study participants. The study was conducted in accordance with the tenets of the Declaration of Helsinki for research involving human subjects and with the Health Insurance Portability and Accountability Act.

All participants had complete ophthalmological examination by a glaucoma specialist (T.C.C.), including history, visual acuity testing, refraction, Goldmann applanation tonometry, slit lamp biomicroscopy, gonioscopy, ultrasonic pachymetry, dilated

ophthalmoscopy, stereo disc photography (Visucam Pro NM; Carl Zeiss Meditec, Inc.), HVF testing (Swedish Interactive Threshold Algorithm or SITA 24-2 standard test of the HVF analyzer 750i; Carl Zeiss Meditec, Inc.), and RNFL thickness scans obtained from the Spectralis OCT (HRA/Spectralis software version 5.4.8.0, Heidelberg Engineering GmbH, Heidelberg, Germany).

Participants were included if they had a spherical equivalent between –5.00 and +5.00 diopters. Only participants with reliable HVF testing, defined as fixation losses ≤33%, false positives ≤20%, and false negatives ≤20%, were included. Participants were excluded if they had congenital anterior chamber abnormalities, corneal opacities or scarring, severe diabetic retinopathy, undilated pupil diameter of 2 mm or less, or HVF loss attributable to a nonglaucoma condition (i.e., retinal scarring, ischemic optic neuropathy, etc.). Only scans with a signal strength of 15 or higher were included. Scans also had to have a clear fundus image during image acquisition and a continuous scan pattern without missing or blank areas. Patients were only included if they were able to have their dilated eye exam and testing (disc photography, HVF testing, SD-OCT testing) on the same day.

Patients with primary open-angle glaucoma, normal tension glaucoma, pseudoexfoliation glaucoma, and pigmentary glaucoma were included if they had best corrected visual acuities of 20/70 or better. The diagnosis of glaucoma was defined as characteristic optic nerve head changes (rim thinning, rim notching, Drance hemorrhages, etc.) with corresponding HVF defects. An HVF was classified as abnormal if three or more contiguous test locations in the pattern standard deviation plot were depressed significantly at the $P < 0.05\%$ level with at least one at the $P < 0.01\%$ level on the same side of the horizontal meridian.[32]

Normal participants were defined as those without ocular diseases except for mild cataracts and those with normal visual field results. Best corrected visual acuity was 20/40 or better. Patients were excluded if they had disc asymmetry greater than 0.2.

Experimental Scan Protocol with Custom-designed Optic Nerve SD-OCT Software

The experimental scan protocol was performed using the Spectralis SD-OCT machine (Heidelberg Engineering, Heidelberg, Germany). It consisted of a 6 × 6 mm, high-density volume scan comprised of 193 B-scans in raster pattern centered over the
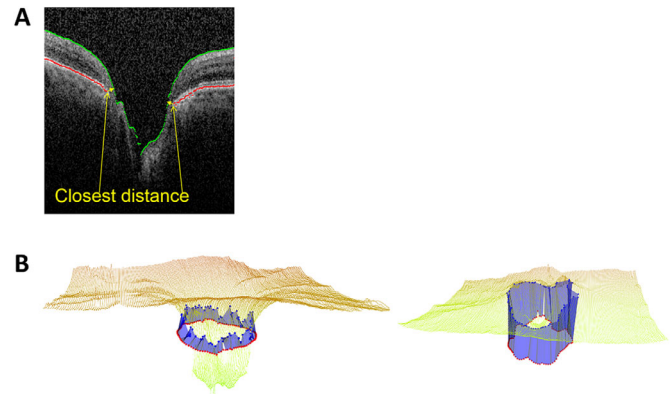
Figure 1. Minimum Distance Band. A) In this B-scan image intersecting the optic nerve head, the yellow arrows indicate the minimum distance band thickness, which represents the shortest distance between the termination of the retinal pigment epithelium/Bruch's membrane complex (red line) and the internal limiting membrane or cup surface (green line) in the plane of the B-scan. B) A three-dimensional rendering of the neuroretinal rim illustrates the minimum distance band area (blue shaded band) in a normal eye (left) and a glaucomatous eye (right).

optic nerve, with an automated real time of three. Raw data was downloaded as a series of images in PNG format. A custom-designed program was coded in C++ using the Open CV, ITK, and VTK libraries (E.T.) to calculate MDB neuroretinal rim parameters. The program automatically segmented the RPE/BM complex and the internal limiting membrane (ILM) in each of the 193 B-scans comprising each volume scan (Fig. 1A). The segmented frames were then individually inspected, and those containing errors in segmentation were manually selected for automatic correction (i.e., interpolation) by the software.

The program identified the optic disc margin based on the termination of the RPE/BM complex, and the margin was represented by 100 circumferential points spaced apart by 3.6° around the optic nerve. MDB neuroretinal rim thickness was defined as the shortest distance between these points and the ILM cup surface. MDB area was calculated by taking two adjacent points on the disc margin and their corresponding nearest points on the cup surface as the vertices of a quadrilateral. The quadrilateral was divided into two triangles, and the area of each triangle was calculated using Heron's formula. The triangle areas were summed. The process was repeated around the disc margin to produce the total MDB area (Fig. 1B). MDB thickness and area were calculated for the overall 360° (global), for 90° quadrants (inferior, superior, nasal, temporal), and for 45° sectors (superior-temporal, superior-nasal, inferior-temporal, inferior-nasal). The program was described in detail previously.[21,22]
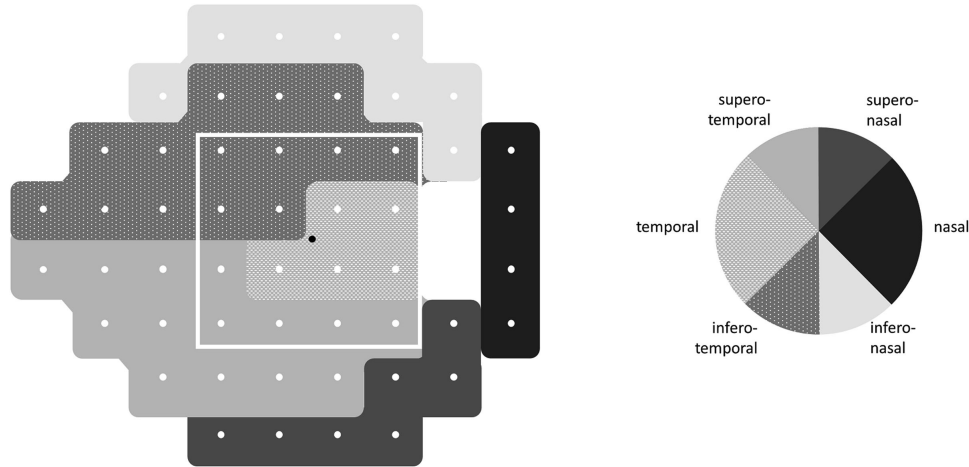
Figure 2. Structure-function correspondence map according to Garway-Heath et al.

Determination of HVF Sensitivities for Structure-Function Correlations

HVF SITA 24-2 total deviation values were recorded for 52 points. These 52 points were grouped into six sections (superior-temporal, superior-nasal, nasal, inferior-nasal, inferior-temporal, and temporal) based on the topographic relationships between visual field locations and corresponding regions of the optic disc as previously described by Garway-Heath et al. (Fig. 2).[28] For this study, HVF total deviation values were converted to a linear scale using the formula $1/\text{Lambert} = (10)^{0.1 \cdot \text{dB}}$ and the average values for each group were calculated. Details can be found elsewhere.[33]

Statistical Analyses

Demographic data for the normal and glaucoma groups were compared using χ^2-test for categorical variables and Student's *t*-test for continuous variables. Logarithmic regression analyses were performed to evaluate the relationship between structural and functional measures globally and in the quadrants and sectors.[34] Pearson correlation coefficients (R) were used to state the strength of the relationships. For comparative purposes only, correlation was defined as strong ($0.80 < R \leq 1.0$), moderate ($0.40 < R \leq 0.80$), or weak ($R \leq 0.40$).[35] A scatter plot with logarithmic fit curve was also generated to show the relationship between visual field total deviation and RNFL thickness/MDB thickness for each quadrant and for each sector. To assess the statistical significance of the difference between the correlation coefficients for MDB thickness and RNFL thickness, Fisher r-to-z transformation online calculator test was used.[36] SAS

statistical software version 9.4 (SAS Institute Inc., Cary, NC) was used for all analyses. Descriptive statistics were reported as mean ± standard deviation (SD). Statistical significance was set at $P < 0.05$. Only one eye per patient was randomly selected using a random number generator statistical table for the analysis.

Results

Characteristics of the Normal and Glaucoma Patients

Of the 102 glaucoma patients, 69 (67.6%) had primary open-angle glaucoma, 13 (12.7%) had normal tension glaucoma, 14 (13.7%) had pseudoexfoliation glaucoma, and 6 (5.9%) had pigmentary glaucoma. The glaucoma group had proportionately fewer females (47 of 102 glaucoma subjects versus 40 of 58 normal subjects, $P = 0.005$, Table 1) and older age (68.1 ± 11.9 years versus 54.3 ± 15.5 years, $P < 0.0001$, Table 1) compared to the normal group. Glaucoma patients also had worse total and mean deviation and higher pattern standard deviation on visual field testing (Table 1). The groups were similar in eye laterality, refractive error, and race.

Correlation Between SD-OCT Structural Parameters and Visual Field Data

Table 2 shows the Pearson correlation coefficients for the relationship between the SD-OCT structural parameters (RNFL thickness, MDB thickness, and MDB area) and the Humphrey visual field data (mean total deviation) for each region in the normal and glaucoma groups. For the glaucoma group,

Table 1. Demographic Characteristics of the Normal and Glaucoma Participants

	Normal	Glaucoma	*P* Value
Number of eyes	58	102	
Number of right eyes/left eyes	32/26	52/50	0.61
Age (years)	54.3 $\pm$ 15.5	68.1 $\pm$ 11.9	<0.0001
Gender (female/male)	40/18	47/55	0.005
Refractive error			
Spherical equivalent (D)	-0.38 ± 1.74	-0.62 ± 1.79	0.42
Visual field[*]			
Total deviation (dB)	-1.16 ± 1.95	-6.87 ± 4.92	<0.0001
Mean deviation (dB)	-1.43 ± 1.93	-11.56 ± 7.40	<0.0001
Pattern standard deviation (dB)	1.52 ± 0.29	8.32 ± 3.24	<0.0001
Race, no. (%)			0.19
Caucasian	38 (65.5)	67 (65.7)	
African-American	8 (13.8)	21 (20.6)	
Hispanic	7 (12.1)	6 (5.9)	
Asian	5 (8.6)	4 (3.9)	
Other[†]	0 (0)	4 (3.9)	

D = diopter; dB = decibel.
[*]Visual field data obtained from Humphrey visual field testing.
[†]Unspecified European descent.
Results are reported as mean $\pm$ standard deviation unless otherwise indicated.

correlations with all three structural parameters were statistically significant for all regions ($P < 0.0001$), except for the MDB area sectors (IN, SN, IT, ST). All correlations, including those for IN, SN, IT, and ST, were weak or moderate. Among the eight quadrants and sectors, the strongest relationships presented in the inferior quadrant for both RNFL thickness ($R = 0.616$) and MDB area ($R = 0.502$) and in the superior quadrant for MDB thickness ($R = 0.559$). However, among the six Garway-Heath regions (i.e., nasal quadrant, temporal quadrant, IN sector, IT sector, SN sector, and ST sector), the strongest relationships presented in the inferior-temporal sector for RNFL thickness ($R = 0.598$), the superior-temporal sector for MDB thickness ($R = 0.531$), and the temporal quadrant for MDB area ($R = 0.450$). For RNFL thickness and MDB thickness, the weakest relationships occurred in the temporal quadrant ($R = 0.348$) and the superior-nasal sector ($R = 0.486$), respectively. There were no statistically significant correlations within the normal group.

Comparison Between RNFL Thickness and MDB Thickness Correlation Coefficients in the Glaucoma Group

In the glaucoma group, RNFL thickness had higher correlation coefficients than MDB thickness in the inferior quadrant and the inferior-temporal sector, while MDB thickness had higher correlation coefficients than RNFL thickness in all other regions. However, these differences were not statistically significant (R values: 0.486 to 0.585 for MDB thickness versus 0.348 to 0.616 for RNFL thickness, $P > 0.05$ for all comparisons).

Regression Between SD-OCT Structural Parameters and Visual Field Data in the Glaucoma Group

Table 3 shows the coefficients of determination (R^2) for the glaucoma group. Among the eight quadrants and sectors, the highest R^2 values were observed in the inferior quadrant for both RNFL thickness ($R^2 = 0.555$) and MDB area ($R^2 = 0.450$) and in the superior quadrant for MDB thickness ($R^2 = 0.491$) (Table 3). Figures 3 and 4 are scatterplots of visual field sensitivity (in dB scale) and RNFL thickness and MDB thickness, respectively. The graphs suggest a curvilinear relationship between the structural and functional measurements with logarithmic fit. Logarithmic regression models showed that all structure-function relationships were statistically significant, except for MDB area sectors (Table 3).

Table 2. Correlation Between Spectral Domain Optical Coherence Tomography Structural Parameters and Humphrey Visual Field Mean Total Deviation for Glaucoma and Normal Patients

	Glaucoma		Normal	
Region	*R* Value[*]	*P* Value	*R* Value[*]	*P* Value
RNFL Thickness				
Overall	0.492	<0.0001	0.088	>0.05
Inferior	0.616	<0.0001	0.109	>0.05
Superior	0.476	<0.0001	−0.027	>0.05
Nasal	0.400	<0.0001	0.190	>0.05
Temporal	0.348	<0.0001	0.033	>0.05
IN	0.521	<0.0001	0.119	>0.05
SN	0.388	<0.0001	−0.159	>0.05
IT	0.598	<0.0001	0.132	>0.05
ST	0.466	<0.0001	0.115	>0.05
MDB Thickness				
Overall	0.585	<0.0001	0.083	>0.05
Inferior	0.536	<0.0001	0.029	>0.05
Superior	0.559	<0.0001	0.061	>0.05
Nasal	0.491	<0.0001	0.029	>0.05
Temporal	0.512	<0.0001	0.059	>0.05
IN	0.528	<0.0001	−0.001	>0.05
SN	0.486	<0.0001	−0.056	>0.05
IT	0.493	<0.0001	0.076	>0.05
ST	0.531	<0.0001	0.135	>0.05
MDB Area				
Overall	0.563	<0.0001	0.030	>0.05
Inferior	0.502	<0.0001	−0.062	>0.05
Superior	0.475	<0.0001	−0.030	>0.05
Nasal	0.427	<0.0001	0.026	>0.05
Temporal	0.450	<0.0001	0.025	>0.05
IN	0.058	0.56	−0.051	>0.05
SN	0.050	0.62	−0.171	>0.05
IT	0.046	0.65	−0.061	>0.05
ST	0.048	0.63	−0.179	>0.05

[*]Pearson correlation coefficients.

RNFL = retinal nerve fiber layer; MDB = minimum distance band; IN = inferior-nasal; SN = superior-nasal; IT = inferior-temporal; ST = superior-temporal.

Discussion

Our data showed that 3D MDB neuroretinal rim thickness correlated with visual field data with similar strength as the most commonly used SD-OCT parameter for glaucoma, peripapillary RNFL thickness. Specifically, RNFL thickness had higher Pearson correlation coefficients than MDB thickness in two out of eight regions, while MDB thickness had higher
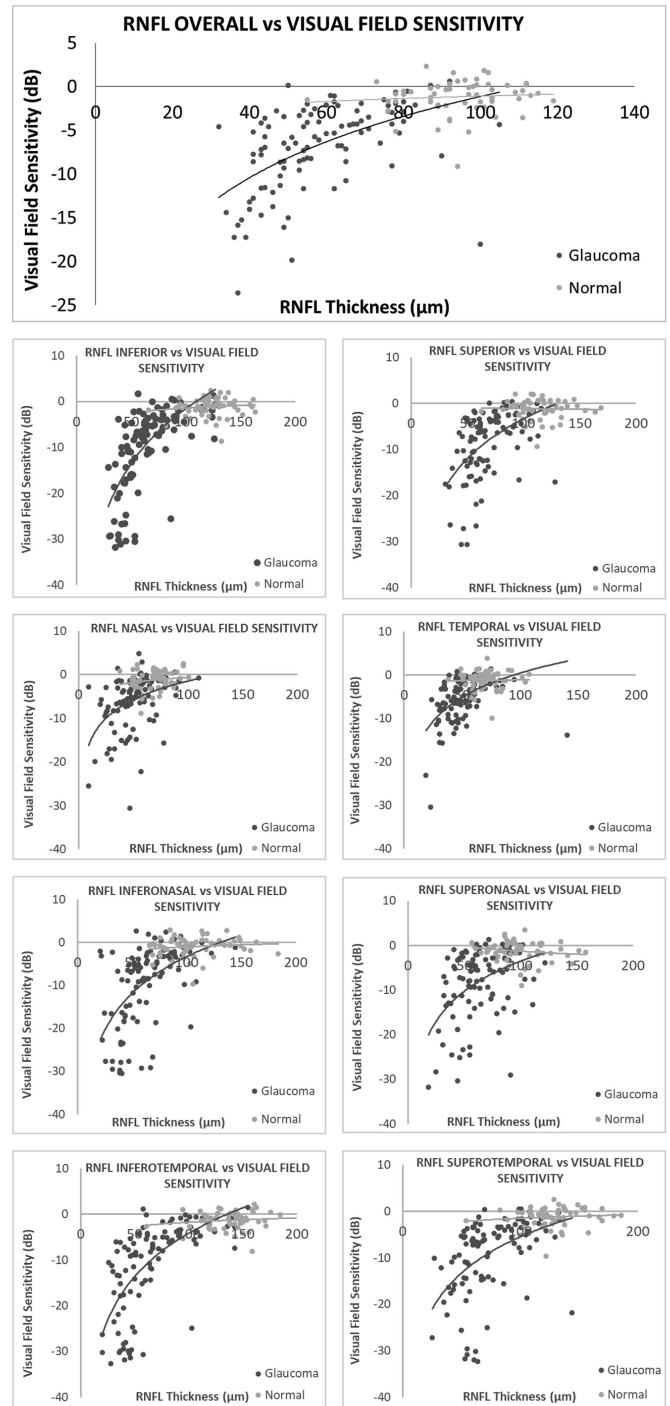
Figure 3. Scatterplot of visual field sensitivity and retinal nerve fiber layer thickness in healthy participants and in patients with glaucoma.

Pearson correlation coefficients in the remaining six out of eight regions (*R*-values ranging from 0.486 to 0.585 for MDB thickness versus 0.348 to 0.616 for RNFL thickness, Table 2), but these differences were not statistically significant (*P* > 0.05 for all comparisons). Our findings align with studies of the structure-function relationship between BMO-MRW

Table 3. Regression Equations Between Spectral-Domain Optical Coherence Tomography Structural Parameters and Visual Field Sensitivity in the Glaucoma Group

Structural Parameter	R^2	$y = a \times \ln(x) + b$	*P* Value
RNFL Thickness			
Overall	0.467	$y = 10.25 \times \ln(x) - 48.07$	<0.0001
Inferior	0.555	$y = 14.05 \times \ln(x) - 68.09$	<0.0001
Superior	0.407	$y = 11.98 \times \ln(x) - 58.38$	<0.0001
Nasal	0.263	$y = 7.07 \times \ln(x) - 32.54$	<0.0001
Temporal	0.313	$y = 8.06 \times \ln(x) - 36.19$	<0.0001
IN	0.401	$y = 12.26 \times \ln(x) - 59.10$	<0.0001
SN	0.300	$y = 10.15 \times \ln(x) - 49.17$	<0.0001
IT	0.546	$y = 12.28 \times \ln(x) - 61.52$	<0.0001
ST	0.394	$y = 11.65 \times \ln(x) - 58.48$	<0.0001
MDB Thickness			
Overall	0.533	$y = 9.40 \times \ln(x) + 9.88$	<0.0001
Inferior	0.476	$y = 12.43 \times \ln(x) + 12.27$	<0.0001
Superior	0.491	$y = 10.65 \times \ln(x) + 10.23$	<0.0001
Nasal	0.351	$y = 8.20 \times \ln(x) + 8.16$	<0.0001
Temporal	0.375	$y = 7.50 \times \ln(x) + 9.15$	<0.0001
IN	0.438	$y = 13.04 \times \ln(x) + 12.26$	<0.0001
SN	0.391	$y = 10.40 \times \ln(x) + 9.30$	<0.0001
IT	0.436	$y = 10.48 \times \ln(x) + 9.91$	<0.0001
ST	0.482	$y = 11.19 \times \ln(x) + 10.80$	<0.0001
MDB Area			
Overall	0.507	$y = 7.68 \times \ln(x) - 6.80$	<0.0001
Inferior	0.450	$y = 9.88 \times \ln(x) + 4.18$	<0.0001
Superior	0.414	$y = 7.85 \times \ln(x) + 2.51$	<0.0001
Nasal	0.307	$y = 6.27 \times \ln(x) + 2.44$	<0.0001
Temporal	0.315	$y = 5.80 \times \ln(x) + 4.12$	<0.0001
IN	0.000	$y = 0.15 \times \ln(x) - 6.32$	0.90
SN	0.001	$y = 0.27 \times \ln(x) - 5.33$	0.79
IT	0.006	$y = 0.98 \times \ln(x) - 5.76$	0.35
ST	0.001	$y = 0.30 \times \ln(x) - 5.87$	0.76

R^2 = coefficient of determination; RNFL = retinal nerve fiber layer; MDB = minimum distance band; IN = inferior-nasal; SN = superior-nasal; IT = inferior-temporal; ST = superior-temporal.

and standard automated perimetry (SAP), which have demonstrated equal or better correlation compared to RNFL thickness and SAP.[8,37–43] This paper is the first to show that MDB thickness, a newer 3D neuroretinal rim parameter derived from high-density volume scans, also relates to glaucomatous vision loss as closely as RNFL thickness measurements and can therefore provide useful structural data to complement functional assessments in glaucoma.

This paper revisits the classic structure-function map developed by Garway-Heath et al. with the latest potential for high-density, 3D SD-OCT imaging of the optic nerve.[29] The Garway-Heath map has been widely adopted in studies of peripapillary RNFL thickness,[2,5,6,8,11,12,44–47] but it was originally designed by tracing RNFL defects to positions of entry at the optic disc.[29] While peripapillary RNFL thickness is measured at a distance from the optic disc, the MDB measures the closest distance from the termination of the RPE/BM complex to the cup surface at the disc itself (Fig. 1A).[21,22] Like the BMO-MRW, it accounts for varying orientation of nerve fibers, and its associated parameter, MDB area, reflects the smallest cross-sectional area through which the nerve fibers must pass as they exit the retina and form the optic nerve. Theoretically, it may therefore be well suited to match
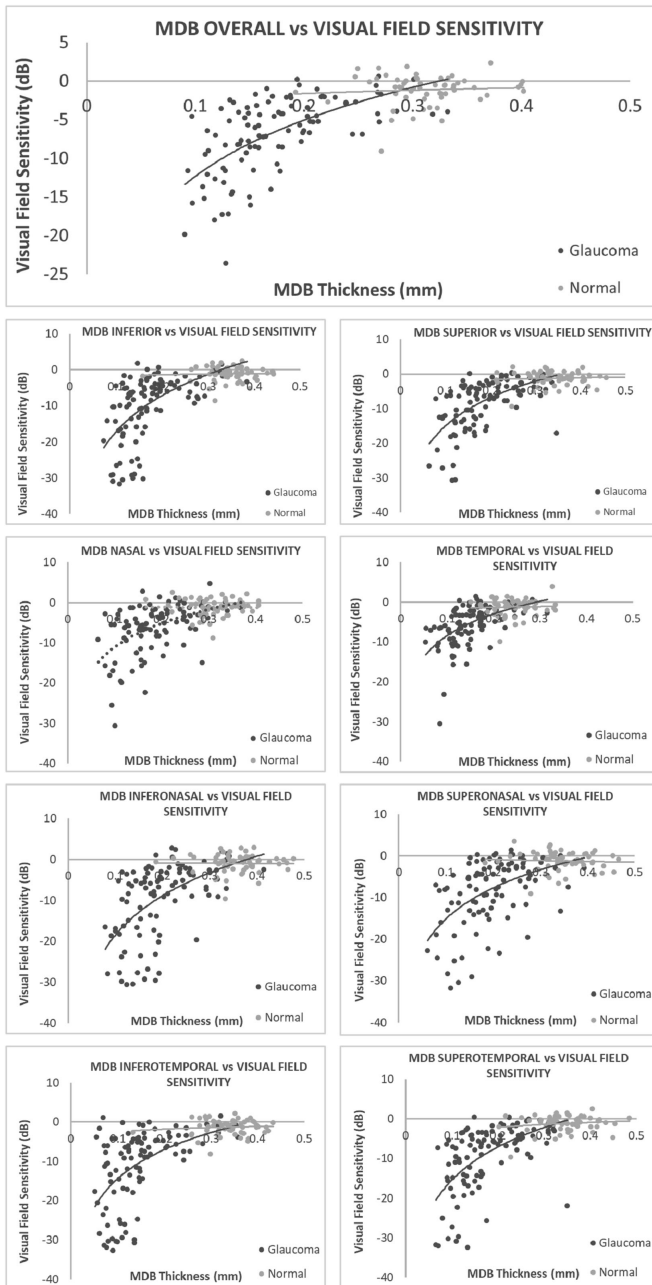
Figure 4. Scatterplot of visual field sensitivity and minimum distance band neuroretinal rim thickness in healthy participants and in patients with glaucoma.

visual field sensitivity changes using the Garway-Heath map.

One might expect 3D MDB neuroretinal rim thickness to reflect functional changes more closely than 2D RNFL thickness for several additional reasons. MDB thickness originates from a high-density volume scan as opposed to a single circular B-scan, allowing for greater reproducibility and fewer artifacts.[21,22] Furthermore, structural changes at the optic nerve can occur prior to RNFL thinning and may therefore accompany early

functional loss better than changes in RNFL thickness.[6,48] Neuroretinal rim thickness may have stronger structure-function correlation in advanced glaucoma as well, as found in a study by Pollet-Villard et al.[8] The investigators attributed the poor RNFL thickness–visual field correlation in advanced glaucoma to the presence of the well-known "floor effect," and hypothesized that neuroretinal rim thickness may have less of a floor effect than RNFL thickness.[8,33,49] In our study, we found higher correlation coefficients for MDB thickness compared to RNFL thickness in six out of eight regions, although these differences were not statistically significant.

For 3D MDB neuroretinal rim thickness, the strongest structure-function relationships among the six Garway-Heath map regions occurred in the superior-temporal sector and the inferior-nasal sector ($R = 0.531$ and 0.528, respectively, Table 2). Several studies using BMO-MRW have also identified the superior-temporal sector as the region with the strongest structure-function relationship, with correlation coefficients ranging from 0.53 to 0.67.[26,42,50] Our data most closely resembles that of Muth et al., who also identified the superior-temporal and inferior-nasal sectors as the two strongest of the six Garway-Heath regions ($R = 0.59$ for both sectors).[26] Alternatively, out of the four quadrants (i.e., superior, inferior, nasal, and temporal), the superior and inferior quadrants had the highest correlations ($R = 0.559$ and 0.536, respectively, Table 2) for MDB thickness. These findings make physiologic sense, as the superior and inferior poles contain the largest rim areas and typically undergo the earliest changes in glaucoma.[51–55] Furthermore, these regions correspond to the most densely sampled regions in SAP; consequently, they are more likely to demonstrate stronger correlation, all other factors being equal.

For 2D peripapillary RNFL thickness, the strongest structure-function relationships among the six Garway-Heath map regions occurred in the inferior-temporal and inferior-nasal sectors ($R = 0.598$ and 0.521, respectively, Table 2). These results are partially at odds with the past two decades of literature on structure-function relationships between RNFL thickness and SAP, which almost uniformly recognize the inferior-temporal and superior-temporal (rather than inferior-nasal) sectors as the two regions with the strongest relationship to visual function (R values ranging from 0.34 to 0.79 for the superior-temporal sector and 0.47 to 0.79 for the inferior-temporal sector).[2,5–12,30,35,42–46,50,56–60] The reason for this partial discrepancy is unclear, although differences across patient populations (e.g., inclusion of normal, preperimetric, and/or ocular hypertension patients),

study methodology (e.g., correlation with threshold sensitivities, total deviation, pattern deviation, or mean deviation), and statistical analyses (e.g., using the linear versus decibel scale for visual field values and linear versus nonlinear regression analyses) may underlie variations in study results. However, consistent with previous research,[2,5,6,8–12,30,35,42–44,47,50,56-58,60,61] we found that the temporal halves of the superior and inferior quadrants each had stronger correlation with visual function than their corresponding nasal halves (R values: ST 0.466 versus SN 0.388 and IT 0.598 versus IN 0.521, Table 2). These results reflect the typical progression of glaucomatous nerve fiber damage, which classically initiates at the superior and inferior optic nerve regions and favor the temporal half of these quadrants.[51-55]

Conversely, we observed the weakest structure-function relationships in the nasal quadrant, superior-nasal sector, and temporal quadrant. For RNFL thickness, the latter two regions were weakest (R values: superior-nasal 0.388 and temporal 0.348, Table 2); for MDB thickness, the former two regions were weakest (R values: nasal 0.491 and superior-nasal 0.486, Table 2). Our results corroborate previous research, which has consistently identified the nasal and temporal quadrants among the weakest correlating regions (R values ranging from 0.05 to 0.49 for the nasal quadrant and 0.01 to 0.46 for the temporal quadrant).[2,5,7,8,10,35,47,57,60,61] These regions have fewer visual field test points, which results in poorer precision and increased variability.[27,62] For example, the region temporal to the blind spot corresponding to the nasal rim has only four test points, as opposed to the inferior-temporal sector, which contains 13 test points. In addition, these quadrants are less commonly affected in early focal glaucoma and are therefore less sensitive for detecting early glaucomatous damage.[52,61,63,64]

Interestingly, the only OCT measurements that showed no significant correlation to visual field sensitivity were the sectoral regions (IN, SN, IT, ST) for MDB area (R values: 0.046 to 0.058, $P > 0.05$ for all sectors, Table 2). These sectors had notably lower Pearson correlation coefficients than all other regions examined. This may be due in part to the smaller sampling size (i.e., sectors comprise one-eighth of the disc circumference as opposed to a quarter or a whole) and the three-dimensional nature of the MDB area measurement. MDB area is calculated by dividing a four-sided region into two triangles that may lie in different planes. It is possible that area measurements are subject to a greater degree of variation than thickness measurements, and therefore, anatomical variation among individual patients may "wash out" corre-

lation in these areas. In contrast, MDB thickness may have a smaller range of variability, allowing for the correlation to persist.

We used total deviation values as our measure of visual field sensitivity loss, as proposed by Hood and Kardon.[33] Many papers have used the raw threshold sensitivity values.[2,6,7,35,42,58,61] However, unlike total deviation, raw threshold values do not account for age-related decreases in visual sensitivity. By using total deviation, we effectively minimize variability in visual sensitivity due to age. On the other hand, RNFL thickness and MDB thickness are not age-adjusted. Nevertheless, data suggest that age has minimal impact on these structural parameters, as RNFL thickness declines by only 0.16 to 0.20 μm per year and MDB thickness by only 3.3% per year.[65–68]

Glaucoma disease severity has been shown to affect structure-function correlation,[34] with a review across papers suggesting stronger relationships in later stages of disease. For example, the relationships between RNFL thickness and SAP measurements reported by Wu et al. ($R = 0.464$ to 0.832, mean MD $= -9.62 \pm 8.68$ dB) were stronger than those reported by Shin et al. ($R = 0.463$ to 0.664, mean MD $= -6.30 \pm 6.57$ dB), and even stronger than those shared by Hirashima et al. ($R = 0.052$ to 0.287, mean MD $= -0.38 \pm 1.35$ dB).[9,10,69] In this study, we reported coefficients of 0.348 to 0.616 for RNFL thickness and SAP in a population with a mean MD of -11.56 ± 7.40 dB, which most closely mirrors that of Wu et al.[10] As with other studies,[3,56,60,69,70] we did not detect a statistically significant structure-function correlation among normal patients, who typically exhibit a smaller range and greater imprecision in structural and functional measurements.[33,60,71]

Our study has limitations. The cross-sectional design does not allow us to elucidate changes in the structure-function relationship over time, which would enhance our understanding of glaucoma progression. Second, we did not include patients with preperimetric glaucoma, and thus our findings cannot extend to this population. It is possible that our decision to include only perimetric glaucoma patients could introduce a selection bias, considering the influence of glaucoma severity on correlation strength, as noted above. On the other hand, their omission narrows the range of data points driving our correlations, and therefore, their absence may have instead led to an underestimate of the strength of the correlations that we reported or negate the selection bias altogether. Third, our glaucoma subjects were identified as those who had characteristic optic nerve changes and corresponding visual field defects; such an enrollment criterion could produce a selection bias toward stronger

structure-function relationship. Lastly, the scans used in our study were taken with the Spectralis software version 5.4.8.0, which has since been updated. Subsequent studies should use the latest software and include a broad range of participants.

The relationship between structural measurements of the optic nerve and measurements of functional vision loss through SAP play an essential role in the diagnosis and management of glaucoma. Our data reveals that 3D MDB neuroretinal rim thickness relates to visual function with similar strength as the most commonly used SD-OCT parameter for glaucoma, 2D peripapillary RNFL thickness, with correlation coefficients ranging from 0.486 to 0.585 for MDB thickness and 0.348 to 0.616 for RNFL thickness ($P > 0.05$ for all comparisons). Prior studies have determined that this newer 3D neuroretinal rim parameter has equal or better diagnostic capability for glaucoma and fewer scan artifacts compared to 2D RNFL thickness.[21,22] Taken together, these findings highlight the advantages of 3D MDB neuroretinal rim thickness in glaucoma care, and future research is needed to uncover its full potential using high-density SD-OCT volume imaging.

Acknowledgments

References

1. Bowd C, Zangwill LM, Berry CC, Blumenthal EZ, Vasile C, Sanchez-Galeana C, Bosworth CF, Sample PA, Weinreb RN. Detecting early glaucoma by assessment of retinal nerve fiber layer thickness and visual function. *Invest Ophthalmol Vis Sci.* 2001;42(9):1993–2003.

2. Aptel F, Sayous R, Fortoul V, Beccat S, Denis P. Structure-function relationships using spectral-domain optical coherence tomography: comparison with scanning laser polarimetry. *Am J Ophthalmol.* 2010;150(6):825–833.

3. Kang EM, Hong S, Kim CY, Seong GJ. Relationship between peripapillary retinal nerve fiber layer thickness measured by optical coherence tomography and visual field severity indices. *Korean J Ophthalmol.* 2015;29(4):263–269.

4. Lee JR, Jeoung JW, Choi J, Choi JY, Park KH, Kim YD. Structure-function relationships in normal and glaucomatous eyes determined by time- and spectral-domain optical coherence tomography. *Invest Ophthalmol Vis Sci.* 2010;51(12):6424–6430.

5. Leite MT, Zangwill LM, Weinreb RN, Rao HL, Alencar LM, Medeiros FA. Structure-function relationships using the Cirrus spectral domain optical coherence tomograph and standard automated perimetry. *J Glaucoma.* 2012;21(1):49–54.

6. Nilforushan N, Nassiri N, Moghimi S, et al. Structure-function relationships between spectral-domain OCT and standard achromatic perimetry. *Invest Ophthalmol Vis Sci.* 2012;53(6):2740–2748.

7. Pinto LM, Costa EF, Melo LA, Jr., et al. Structure-function correlations in glaucoma using matrix and standard automated perimetry versus time-domain and spectral-domain OCT devices. *Invest Ophthalmol Vis Sci.* 2014;55(5):3074–3080.

8. Pollet-Villard F, Chiquet C, Romanet JP, Noel C, Aptel F. Structure-function relationships with spectral-domain optical coherence tomography retinal nerve fiber layer and optic nerve head measurements. *Invest Ophthalmol Vis Sci.* 2014;55(5):2953–2962.

9. Shin HY, Park HY, Jung KI, Park CK. Comparative study of macular ganglion cell-inner plexiform layer and peripapillary retinal nerve fiber layer measurement: structure-function analysis. *Invest Ophthalmol Vis Sci.* 2013;54(12):7344–7353.

10. Wu H, de Boer JF, Chen L, Chen TC. Correlation of localized glaucomatous visual field defects and spectral domain optical coherence tomography retinal nerve fiber layer thinning using a modified structure-function map for OCT. *Eye (Lond).* 2015;29(4):525–533.

11. Kanamori A, Nakamura M, Tomioka M, Kawaka Y, Yamada Y, Negi A. Structure-function relationship among three types of spectral-domain

optical coherent tomography instruments in measuring parapapillary retinal nerve fibre layer thickness. *Acta Ophthalmol.* 2013;91(3):e196–e202.

12. Rao HL, Zangwill LM, Weinreb RN, Leite MT, Sample PA, Medeiros FA. Structure-function relationship in glaucoma using spectral-domain optical coherence tomography. *Arch Ophthalmol.* 2011;129(7):864–871.

13. Asrani S, Essaid L, Alder BD, Santiago-Turla C. Artifacts in spectral-domain optical coherence tomography measurements in glaucoma. *JAMA Ophthalmol.* 2014;132(4):396–402.

14. Liu Y, Simavli H, Que CJ, et al. Patient characteristics associated with artifacts in Spectralis optical coherence tomography imaging of the retinal nerve fiber layer in glaucoma. *Am J Ophthalmol.* 2015;159(3):565–576.e562.

15. Choi S JF, Tsikata E, Khoueir Z, et al. Artifact rates for 2D retinal nerve fiber layer thickness versus 3D retinal nerve fiber layer volume. *Trans Vis Sci Tech.* 2020;9(3):12.

16. Ashimatey BS, Swanson WH. Between-subject variability in healthy eyes as a primary source of structural-functional discordance in patients with glaucoma. *Invest Ophthalmol Vis Sci.* 2016;57(2):502–507.

17. Simavli H, Poon LY, Que CJ, et al. Diagnostic capability of peripapillary retinal volume measurements in laucoma. *J Glaucoma.* 2017;26(6):592–601.

18. Chauhan BC, O'Leary N, AlMobarak FA, et al. Enhanced detection of open-angle glaucoma with an anatomically accurate optical coherence tomography-derived neuroretinal rim parameter. *Ophthalmology.* 2013;120(3):535–543.

19. Gardiner SK, Ren R, Yang H, Fortune B, Burgoyne CF, Demirel S. A method to estimate the amount of neuroretinal rim tissue in glaucoma: comparison with current methods for measuring rim area. *Am J Ophthalmol.* 2014;157(3):540–549.e541–e542.

20. Gmeiner JM, Schrems WA, Mardin CY, Laemmer R, Kruse FE, Schrems-Hoesl, LM. Comparison of Bruch's membrane opening minimum rim width and peripapillary retinal nerve fiber layer thickness in early glaucoma assessment. *Invest Ophthalmol Vis Sci.* 2016;57(9):OCT575–OCT584.

21. Shieh E, Lee R, Que C, et al. Diagnostic performance of a novel three-dimensional neuroretinal rim parameter for glaucoma using high-density volume scans. *Am J Ophthalmol.* 2016;169:168–178.

22. Tsikata E, Lee R, Shieh E, et al. Comprehensive three-dimensional analysis of the neuroretinal rim in glaucoma using high-density spectral-domain optical coherence tomography volume scans. *Invest Ophthalmol Vis Sci.* 2016;57(13):5498–5508.

23. Chen TC. Spectral domain optical coherence tomography in glaucoma: qualitative and quantitative analysis of the optic nerve head and retinal nerve fiber layer (an AOS thesis). *Trans Am Ophthalmol Soc.* 2009;107:254–281.

24. Povazay B, Hofer B, Hermann B, et al. Minimum distance mapping using three-dimensional optical coherence tomography for glaucoma diagnosis. *J Biomed Opt.* 2007;12(4):041204.

25. Chauhan BC, Burgoyne CF. From clinical examination of the optic disc to clinical assessment of the optic nerve head: a paradigm change. *Am J Ophthalmol.* 2013;156(2):218–227 e212.

26. Muth DR, Hirneiss CW. Structure-function relationship between Bruch's membrane opening-based optic nerve head parameters and visual field defects in glaucoma. *Invest Ophthalmol Vis Sci.* 2015;56(5):3320–3328.

27. Garway-Heath DF, Caprioli J, Fitzke FW, Hitchings RA. Scaling the hill of vision: the physiological relationship between light sensitivity and ganglion cell numbers. *Invest Ophthalmol Vis Sci.* 2000;41(7):1774–1782.

28. Garway-Heath DF, Holder GE, Fitzke FW, Hitchings RA. Relationship between electrophysiological, psychophysical, and anatomical measurements in glaucoma. *Invest Ophthalmol Vis Sci.* 2002;43(7):2213–2220.

29. Garway-Heath DF, Poinoosawmy D, Fitzke FW, Hitchings RA. Mapping the visual field to the optic disc in normal tension glaucoma eyes. *Ophthalmology.* 2000;107(10):1809–1815.

30. Kanamori A, Naka M, Nagai-Kusuhara A, Yamada Y, Nakamura M, Negi A. Regional relationship between retinal nerve fiber layer thickness and corresponding visual field sensitivity in glaucomatous eyes. *Arch Ophthalmol.* 2008;126(11):1500–1506.

31. Wirtschafter JD, Becker WL, Howe JB, Younge BR. Glaucoma visual field analysis by computed profile of nerve fiber function in optic disc sectors. *Ophthalmology.* 1982;89(3):255–267.

32. Simavli H, Que CJ, Akduman M, et al. Diagnostic capability of peripapillary retinal thickness in glaucoma using 3D volume scans. *Am J Ophthalmol.* 2015;159(3):545–556 e542.

33. Hood DC, Kardon RH. A framework for comparing structural and functional measures of glaucomatous damage. *Prog Retin Eye Res.* 2007;26(6):688–710.

translational vision science & technology

34. Leung CK, Chong KK, Chan WM, et al. Comparative study of retinal nerve fiber layer measurement by StratusOCT and GDx VCC, II: structure/function regression analysis in glaucoma. *Invest Ophthalmol Vis Sci.* 2005;46(10):3702–3711.

35. Leaney J, Healey PR, Lee M, Graham SL. Correlation of structural retinal nerve fibre layer parameters and functional measures using Heidelberg Retinal Tomography and Spectralis spectral domain optical coherence tomography at different levels of glaucoma severity. *Clin Exp Ophthalmol.* 2012;40(8):802–812.

36. Significance of the difference between two correlation coefficients. VassarStats website. Accessed May 14, 2021, http://vassarstats.net/rdiff.html.

37. Danthurebandara VM, Sharpe GP, Hutchison DM, et al. Enhanced structure-function relationship in glaucoma with an anatomically and geometrically accurate neuroretinal rim measurement. *Invest Ophthalmol Vis Sci.* 2014;56(1):98–105.

38. Enders P, Schaub F, Adler W, et al. Bruch's membrane opening-based optical coherence tomography of the optic nerve head: a useful diagnostic tool to detect glaucoma in macrodiscs. *Eye (Lond).* 2018;32(2):314–323.

39. Enders P, Schaub F, Adler W, Nikoluk R, Hermann MM, Heindl LM. The use of Bruch's membrane opening-based optical coherence tomography of the optic nerve head for glaucoma detection in microdiscs. *Br J Ophthalmol.* 2017;101(4):530–535.

40. Imamoglu S, Celik NB, Sevim MS, et al. Structure-function relationship between the Bruch membrane opening-based minimum rim width and visual field defects in advanced glaucoma. *J Glaucoma.* 2017;26(6):561–565.

41. Lopes FS, Matsubara I, Almeida I, et al. Structure-function relationships in glaucoma using enhanced depth imaging optical coherence tomography-derived parameters: a cross-sectional observational study. *BMC Ophthalmol.* 2019;19(1):52.

42. Mizumoto K, Gosho M, Zako M. Correlation between optic nerve head structural parameters and glaucomatous visual field indices. *Clin Ophthalmol.* 2014;8:1203–1208.

43. Reznicek L, Muth D, Vogel M, Hirneiss C. Structure-function relationship between flicker-defined form perimetry and spectral-domain optical coherence tomography in glaucoma suspects. *Curr Eye Res.* 2017;42(3):418–423.

44. Amini N, Daneshvar R, Sharifipour F, et al. Structure-function relationships in perimetric glaucoma: comparison of minimum-rim width and retinal nerve fiber layer parameters. *Invest Ophthalmol Vis Sci.* 2017;58(11):4623–4631.

45. Ballae Ganeshrao S, Turpin A, Denniss J, McKendrick AM. Enhancing structure-function correlations in glaucoma with customized spatial mapping. *Ophthalmology.* 2015;122(8):1695–1705.

46. Horn FK, Mardin CY, Laemmer R, et al. Correlation between local glaucomatous visual field defects and loss of nerve fiber layer thickness measured with polarimetry and spectral domain OCT. *Invest Ophthalmol Vis Sci.* 2009;50(5):1971–1977.

47. Takagishi M, Hirooka K, Baba T, Mizote M, Shiraga F. Comparison of retinal nerve fiber layer thickness measurements using time domain and spectral domain optical coherence tomography, and visual field sensitivity. *J Glaucoma.* 2011;20(6):383–387.

48. Strouthidis NG, Fortune B, Yang H, Sigal IA, Burgoyne CF. Longitudinal change detected by spectral domain optical coherence tomography in the optic nerve head and peripapillary retina in experimental glaucoma. *Invest Ophthalmol Vis Sci.* 2011;52(3):1206–1219.

49. Leung CK, Cheung CY, Weinreb RN, et al. Evaluation of retinal nerve fiber layer progression in glaucoma: a study on optical coherence tomography guided progression analysis. *Invest Ophthalmol Vis Sci.* 2010;51(1):217–222.

50. Reznicek L, Burzer S, Laubichler A, et al. Structure-function relationship comparison between retinal nerve fibre layer and Bruch's membrane opening-minimum rim width in glaucoma. *Int J Ophthalmol.* 2017;10(10):1534–1538.

51. Hood DC, Wang DL, Raza AS, de Moraes CG, Liebmann JM, Ritch R. The locations of circumpapillary glaucomatous defects seen on frequency-domain OCT scans. *Invest Ophthalmol Vis Sci.* 2013;54(12):7338–7343.

52. Jonas JB, Fernandez MC, Sturmer J. Pattern of glaucomatous neuroretinal rim loss. *Ophthalmology.* 1993;100(1):63–68.

53. Leung CK, Choi N, Weinreb RN, et al. Retinal nerve fiber layer imaging with spectral-domain optical coherence tomography: pattern of RNFL defects in glaucoma. *Ophthalmology.* 2010;117(12):2337–2344.

54. Quigley HA, Green WR. The histology of human glaucoma cupping and optic nerve damage: clinicopathologic correlation in 21 eyes. *Ophthalmology.* 1979;86(10):1803–1830.

55. Tuulonen A, Airaksinen PJ. Initial glaucomatous optic disk and retinal nerve fiber layer abnormalities and their progression. *Am J Ophthalmol.* 1991;111(4):485–490.

56. Alnawaiseh M, Homberg L, Eter N, Prokosch V. Comparison between the correlations of retinal nerve fiber layer thickness measured by spectral domain optical coherence tomography and visual field defects in standard automated white-on-white perimetry versus pulsar perimetry. *J Ophthalmol.* 2017;2017:8014294.

57. Lamparter J, Russell RA, Schulze A, Schuff AC, Pfeiffer N, Hoffmann EM. Structure-function relationship between FDF, FDT, SAP, and scanning laser ophthalmoscopy in glaucoma patients. *Invest Ophthalmol Vis Sci.* 2012;53(12):7553–7559.

58. Bowd C, Zangwill LM, Medeiros FA, et al. Structure-function relationships using confocal scanning laser ophthalmoscopy, optical coherence tomography, and scanning laser polarimetry. *Invest Ophthalmol Vis Sci.* 2006;47(7):2889–2895.

59. Kita Y, Hollomicron G, Saito T, Murai A, Kita R, Hirakata A. Circumpapillary microperimetry to detect glaucoma: a pilot study for sector-based comparison to circumpapillary retinal nerve fiber layer measurement. *Int Ophthalmol.* 2019; 39(1):127–136.

60. Miglior S, Riva I, Guareschi M, et al. Retinal sensitivity and retinal nerve fiber layer thickness measured by optical coherence tomography in glaucoma. *Am J Ophthalmol.* 2007;144(5):733–740.

61. Monsalve B, Ferreras A, Khawaja AP, et al. The relationship between structure and function as measured by OCT and Octopus perimetry. *Br J Ophthalmol.* 2015;99(9):1230–1235.

62. Budenz DL, Chang RT, Huang X, Knighton RW, Tielsch JM. Reproducibility of retinal nerve fiber thickness measurements using the stratus OCT in normal and glaucomatous eyes. *Invest Ophthalmol Vis Sci.* 2005;46(7):2440–2443.

63. Hood DC, Raza AS, de Moraes CG, Johnson CA, Liebmann JM, Ritch R. The Nature of macular damage in glaucoma as revealed by averaging optical coherence tomography data. *Transl Vis Sci Technol.* 2012;1(1):3.

64. Kanamori A, Nakamura M, Escano MF, Seya R, Maeda H, Negi A. Evaluation of the glaucomatous damage on retinal nerve fiber layer thickness measured by optical coherence tomography. *Am J Ophthalmol.* 2003;135(4):513–520.

65. Budenz DL, Anderson DR, Varma R, et al. Determinants of normal retinal nerve fiber layer thickness measured by Stratus OCT. *Ophthalmology.* 2007;114(6):1046–1052.

66. Knight OJ, Girkin CA, Budenz DL, Durbin MK, Feuer WJ, Cirrus OCTNDSG. Effect of race, age, and axial length on optic nerve head parameters and retinal nerve fiber layer thickness measured by Cirrus HD-OCT. *Arch Ophthalmol.* 2012;130(3):312–318.

67. Parikh RS, Parikh SR, Sekhar GC, Prabakaran S, Babu JG, Thomas R. Normal age-related decay of retinal nerve fiber layer thickness. *Ophthalmology.* 2007;114(5):921–926.

68. Poon LY, Antar H, Tsikata E, et al. Effects of age, race, and ethnicity on the optic nerve and peripapillary region using spectral-domain OCT 3D volume scans. *Transl Vis Sci Technol.* 2018;7(6):12.

69. Hirashima T, Hangai M, Nukada M, et al. Frequency-doubling technology and retinal measurements with spectral-domain optical coherence tomography in preperimetric glaucoma. *Graefes Arch Clin Exp Ophthalmol.* 2013;251(1):129–137.

70. Naghizadeh F, Garas A, Vargha P, Hollo G. Structure-function relationship between the octopus perimeter cluster mean sensitivity and sector retinal nerve fiber layer thickness measured with the RTVue optical coherence tomography and scanning laser polarimetry. *J Glaucoma.* 2014;23(1):11–18.

71. Ajtony C, Balla Z, Somoskeoy S, Kovacs B. Relationship between visual field sensitivity and retinal nerve fiber layer thickness as measured by optical coherence tomography. *Invest Ophthalmol Vis Sci.* 2007;48(1):258–263.